J.D. Biggs, A. Negri
Orbit-Attitude Control in a Circular Restricted Three-Body Problem Using Distributed Reflectivity Devices
Journal of Guidance Control and Dynamics, In press - Published online 21/08/2019
doi:10.2514/1.G004493

Orbit-attitude control in a circular restricted three-body problem using distributed reflectivity devices

James D. Biggs * and Alessio Negri †
Politecnico di Milano, Milan, Italy

I. Introduction

Solar sail spacecraft utilize their large surface areas to reflect photons emitted from the Sun to generate a resultant force and torque. One of the advantages of solar sail propulsion is that they can generate unique orbits, known as highly non-Keplerian orbits, for long durations [1]. Solar sail non-Keplerian orbits can enable a wide range of new space applications, including pole-sitters [2] and early warning solar storm missions such as the Sunjammer [3]. These non-Keplerian orbits are initially designed using the assumption of a fixed angle between the solar sail normal and the Sun direction. However, these orbits are highly unstable and require station-keeping using closed-loop control. Control actuation of solar sail spacecraft can be achieved by varying its surface area, reflectivity properties [4–7] and force-vectoring through attitude control [8–11].

Station-keeping in the vicinity of libration point orbits has used linear feedback-control that requires continuous time-varying attitude re-orientations to ensure asymptotic stability of the closed-loop linearized system [8–11]. Station-keeping in solar sail restricted three body problems tend to assume that the solar sail can match the required attitude exactly. However, solar sail attitude control is non-trival since conventional actuation is not suitable; thrusters use fuel and so are not useful for long duration missions, while reaction wheels would require thrusters for de-saturation. Furthermore, reaction wheels may experience significant wear and tear over long duration missions, with increased jitter and friction. Therefore, solar sails need to employ unconventional methods for attitude control. Wie [12, pp. 767-774] analyzed the use of a two-axis gimbaled control boom in order to shift the center-of-pressure with respect to the center-of-mass to induce a required torque. In addition, four control vanes are proposed for 3-axis attitude control placed at the corners of a square sail. Takao et al. [13] proposed actuation by actively deforming the sail membrane to generate both torques and forces. As demonstrated on the solar sail IKAROS, reflectivity control devices (RCDs) can also provide a novel actuation method for attitude control [14].

An RCD is a thin film device capable of controlling the orientation of liquid crystal components, placed in between two electrodes at which a certain voltage is applied. As a result, the reflectivity characteristic of the device can switch between two different states, such as diffusive to specular reflection or absorption to specular reflection. The concept of using RCDs has been demonstrated for deep-space orbit control in [4–7] and for orbit-attitude control in the vicinity

*Associate Professor, Department of Aerospace Science and Technology, jamesdouglas.biggs@polimi.it.
†Graduate Student, MSc Space Engineering, Department of Aerospace Science and Technology, alessio1.negri@mail.polimi.it.

of libration points in [6, 7]. In these cases the sail surface is assumed to be a continuum of RCDs with the ability to provide a continuous control between a maximum and minimum value. A more practically viable case is considered in [15], where the sail surface consists of a finite number of RCDs each having the capability to switch between reflection and absorption for attitude control. The attitude control algorithm in [15] is based on mapping a proportional feedback law, to either an ON or OFF state of each RCD, such that the vector norm between the ideal and generated torque is minimized. However, for N-RCDs, the algorithm becomes computationally expensive, with 2^N possible combinations to consider. Moreover, as the number of RCDs increases the ratio of the number of possible torques to the number of possible combinations decreases exponentially. For example, with 16 RCDs there are 65,536 possible combinations with the number of possible torques only 0.6% of the number of possible ON-OFF combinations. Thus, using this approach it is computationally expensive to increase the precision of the control by introducing a greater range of torques through an increased number of RCDs.

This paper uses the distributed RCDs attitude control concept posed in [15] and extends it to coupled orbit-attitude control in the circular restricted three body problem (CR3BP). The proposed RCD allocation procedure also massively decreases the amount of computations required for high-precision tracking. In addition, the solar radiation pressure is modelled in its full vectorial form, without the assumption that it only acts in the sail plane. The RCDs are assumed to switch between a specular and an absorptive state offering a wider range of torque magnitudes compared to diffusive-to-specular switching [4, 6]. Our approach is to project ideal continuous forces and torques (ideal as they are computed using feedback controls that do not consider the mechanism of actuation), onto the ON or OFF state of each RCD. The ideal force and torques are generated by coupling an LQR orbit control with an attitude bore-sight control [16]. The procedure for projecting the ideal control onto each RCD exploits the symmetry of the sail and uses a convenient analytical formula for the torque in terms of the centre-of-pressure and ON-OFF combinations of the RCDs.

II. Orbit-attitude solar sail dynamics

In this section we introduce the solar radiation pressure model and the RCD control mechanism. These force and torque models are incorporated into the six-degree of freedom orbit-attitude dynamics.

A. Solar Radiation Pressure

The expression of the solar radiation pressure (SRP) can be derived either from quantum mechanics or electromagnetic theory [17, pp. 34-38]. The SRP force vector $\mathbf{F}$ is given by Ref. [12, pp. 749-752]

$$\mathbf{F} = P\ S < \mathbf{s}, \mathbf{n} > [(\rho_a + \rho_d)\ \mathbf{s} + (2\ \rho_s < \mathbf{s}, \mathbf{n} > + 2/3\ \rho_d)\ \mathbf{n}] \tag{1}$$

where $\mathbf{F}$ is the SRP force vector, $P = P_0/r^2$ is the SRP ($P_0 = 4.56 \times 10^{-6}\,\mathrm{N\,m^{-2}}$), S is the sail surface area, $\mathbf{s}$ is the Sun direction (pointing away from the Sun), $\mathbf{n}$ is the sail normal and $< \cdot, \cdot >$ is the scalar product. This model considers the specular reflectivity coefficient (ρ_s), the diffuse reflectivity coefficient (ρ_d) and the absorptivity coefficient (ρ_a) where $\rho_s + \rho_d + \rho_a = 1$. Due to the nature of the RCD (similarly to that used on IKAROS) it can switch between a specular state (i.e., ON coefficients $\rho_s^{ON} = 1$,$\rho_a^{ON} = 0$) and an absorptive state ($\rho_s^{OFF} = 0$, $\rho_a^{OFF} = 1$). It is assumed that the device has no diffuse reflectivity such that $\rho_d = 0$. With the selected logic, Equation 1 can be simplified to

$$\mathbf{F} = P\,S < \mathbf{s}, \mathbf{n} > [(1 - \rho_s)\,\mathbf{s} + 2\,\rho_s < \mathbf{s}, \mathbf{n} > \mathbf{n}] \tag{2}$$

Note that this model induces a force along the sail normal ($\mathbf{n}$) and the Sun direction ($\mathbf{s}$) as shown in Fig. 1. For an ideal sail ($\rho_s = 1$) the angle between the Sun direction and the sail normal is called the cone angle α and the force acts along the sail normal. Instead, the resultant force in this model acts along $\mathbf{m}$ which forms an angle $\theta \leq \alpha$ with the Sun direction, called the effective cone angle. If the force is expressed as the sum of the perpendicular ($\mathbf{n}$) and tangent ($\mathbf{t}$) force, the relation between the two angles becomes

$$\alpha - \theta = \arctan\left(\frac{1 - \rho_s}{1 + \rho_s}\,\tan\alpha\right) \tag{3}$$

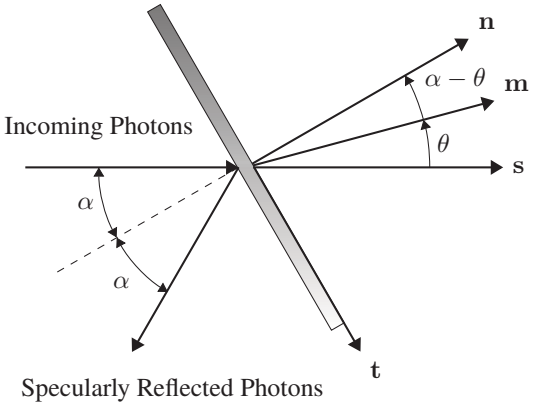

Fig. 1 Solar radiation pressure geometry.

B. Attitude Dynamics and Kinematics

To introduce the attitude dynamics and kinematics we define an inertial reference frame $N = [X_N : Y_N : Z_N]$ fixed in the Sun-Earth barycentre, with Z_N normal to the ecliptic plane containing the two main bodies, X_N pointing toward the Ares point, while Y_N completes the right-handed orthonormal frame. The solar sail body-fixed frame $B = [X_B : Y_B : Z_B]$ is defined such that X_B is aligned with the sail normal $\mathbf{n}_B$ in body fixed coordinates, and Y_B and Z_B lie in the sail plane fixed at its geometric centre.

Assuming a symmetric solar sail ($J_y = J_z = J$) and no significant disturbance apart from SRP (as is the case at the libration point orbit) the attitude dynamics can be written as

$$\begin{cases} J_x\,\dot{\omega}_x &= u_x \\ J\,\dot{\omega}_y &= (J - J_x)\,\omega_z\,\omega_x + u_y \\ J\,\dot{\omega}_z &= (J_x - J)\,\omega_x\,\omega_y + u_z \end{cases} \tag{4}$$

where J_j represent the principal moments of inertia, ω_j are the components of the angular velocity of the body frame B with respect to an inertial frame N and u_j are the torque components ($j = x, y, z$) where from Eq. 2 we have

$$\begin{cases} u_x &= P\,S\,\cos^2\alpha\,\tan\alpha\,(Z\,\cos\gamma + Y\,\sin\gamma)\,(1 - \rho_s) \\ u_y &= P\,S\,\cos^2\alpha\,Z\,(1 + \rho_s) \\ u_z &= -P\,S\,\cos^2\alpha\,Y\,(1 + \rho_s) \end{cases} \tag{5}$$

where (Y, Z) are the coordinates of the center of pressure with respect to the center of the sail (i.e., center of mass) and where γ is the roll angle as shown in Figure 2 and will be defined precisely in the next section. The SRP torque is generated by an offset between the center-of-pressure and the center-of-mass.

The kinematics are expressed in quaternions $\mathbf{q}$ of the body-fixed frame with respect to the inertial frame

$$\dot{\mathbf{q}} = \frac{1}{2}\mathbf{q} \otimes \boldsymbol{\omega} \tag{6}$$

where $\otimes$ represents the quaternion product and $\boldsymbol{\omega} = [\omega_x \quad \omega_y \quad \omega_z]^T$ is the angular velocity vector of the frame B with respect N.

C. Solar Sail Circular Restricted Three-Body Problem

The orbital dynamics of the solar sail is modelled in the CR3BP where the two primarues are the Sun and Earth perturbed by solar radiation pressure. The dynamics of the solar sail is expressed in the synodic frame $Sy = [\hat{i} : \hat{j} : \hat{k}]$ in which the origin is at the barycentre of of the Sun-Earth system. The unit vector $\hat{i}$ is directed along the Sun to Earth line and the unit vector $\hat{k}$ is parallel to the angular momentum vector of the Earth and the unit vector $\hat{j}$ completes the

right handed orthonormal frame. The solar sail dynamics are then expressed as:

$$\begin{cases} \ddot{x} - 2\dot{y} &= \frac{\partial U}{\partial x} + a_x \\ \ddot{y} + 2\dot{x} &= \frac{\partial U}{\partial y} + a_y \\ \ddot{z} &= \frac{\partial U}{\partial z} + a_z \end{cases} \tag{7}$$

where $\boldsymbol{r} = x\hat{i} + y\hat{j} + z\hat{k}$ is the non-dimensional position vector of the sail, a_x, a_y, a_z are the components of the SRP acceleration and U is the pseudo-potential function:

$$U = \frac{(1-\mu)}{||\mathbf{r}_1||} + \frac{\mu}{||\mathbf{r}_2||} + \frac{1}{2}\,(x^2 + y^2), \tag{8}$$

with μ defined as the mass ratio. Where $\mathbf{r}_1 = [(x+\mu) \quad y \quad z]^T$ is the position of the sail with respect to the Sun and $\mathbf{r}_2 = [(x-(1-\mu)) \quad y \quad z]^T$ is the position of the sail with respect to the Earth. To define the attitude dependent solar sail acceleration we define a reference frame $L = [X_L : Y_L : Z_L]$ fixed at geometric centre of the sail. Here X_L is directed along the Sun direction $\hat{\mathbf{r}}_1$, Z_L is defined to be perpendicular to X_L and $\hat{\mathbf{k}}$ and Y_L completes the right-handed orthonormal frame as shown in Fig. 2. The cone angle α is the angle between the sail normal $\mathbf{n}_B$ and the Sun direction $X_L \equiv \hat{\mathbf{r}}_1$, while δ is the angle between Y_L and the projection of the normal of the sail on to the plane (Y_L, Z_L). γ is the angle of the roll axis of the sail, but this does not effect the orbit acceleration.

At this point the expression for the SRP acceleration has to be introduced. The model selected considers the sail with both specular reflective and absorptive characteristics (derived from Eq. 2). First consider the expression of the sail normal in S

$$\begin{cases} n_x &= \frac{\cos\alpha\ (x+\mu)}{\|\mathbf{r}_1\|} - \frac{\sin\alpha\ \cos\delta\ (x+\mu)\ z}{\|(\mathbf{r}_1\times\hat{\mathbf{k}})\times\mathbf{r}_1\|} + \frac{\sin\alpha\ \sin\delta\ y}{\|\mathbf{r}_1\times\hat{\mathbf{k}}\|} \\ n_y &= \frac{\cos\alpha\ y}{\|\mathbf{r}_1\|} - \frac{\sin\alpha\ \cos\delta\ y\ z}{\|(\mathbf{r}_1\times\hat{\mathbf{k}})\times\mathbf{r}_1\|} - \frac{\sin\alpha\ \sin\delta\ (x+\mu)}{\|\mathbf{r}_1\times\hat{\mathbf{k}}\|} \\ n_z &= \frac{\cos\alpha\ z}{\|\mathbf{r}_1\|} + \frac{\sin\alpha\ \cos\delta\ (y^2+(x+\mu)^2)}{\|(\mathbf{r}_1\times\hat{\mathbf{k}})\times\mathbf{r}_1\|} \end{cases} \tag{9}$$

where $\mathbf{r}_1$ is the Sun-sail position vector, $\|\cdot\|$ is the norm of a vector and $\cdot\times\cdot$ is the vector product. As a result, the components of the acceleration can be derived

$$\begin{cases} a_x &= \rho_s\ \beta\ \frac{1-\mu}{r_1^2}\ \cos^2\alpha\ n_x + \frac{(1-\rho_s)}{2}\ \beta\ \frac{1-\mu}{r_1^3}\ \cos\alpha\ (x+\mu) \\ a_y &= \rho_s\ \beta\ \frac{1-\mu}{r_1^2}\ \cos^2\alpha\ n_y + \frac{(1-\rho_s)}{2}\ \beta\ \frac{1-\mu}{r_1^3}\ \cos\alpha\ y \\ a_z &= \rho_s\ \beta\ \frac{1-\mu}{r_1^2}\ \cos^2\alpha\ n_z + \frac{(1-\rho_s)}{2}\ \beta\ \frac{1-\mu}{r_1^3}\ \cos\alpha\ z \end{cases} \tag{10}$$

where r_1 is the norm of $\mathbf{r}_1$ and β is the sail lightness parameter defined as the ratio of the critical sail loading parameter

$\sigma^* = 1.53\,\mathrm{g\,m^{-2}}$ and the sail loading parameter $\sigma = m/S$ (with m the mass of the sail).

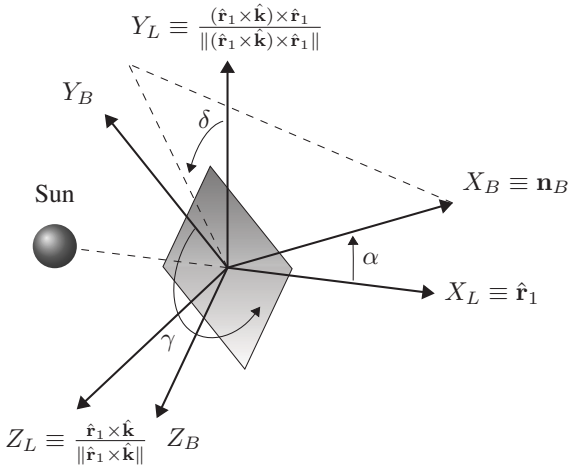

Fig. 2 Rotating L and body-fixed B frames.

III. Ideal Controls

In this section the ideal controls used to generate the continuous force and torque signals that will be distributed to the RCDs are described. These controls are developed independently for the orbit and attitude dynamics, but provide forces and torques that depend on the current state. The goal is then to match these ideal forces and torques as closely as possible using combinations of the on-off switching of each RCD.

A. Non-ideal solar sail control in the vicinity of artificial equilibrium points (AEP)

The objective of this paper is to develop the coupled orbit-attitude control using RCDs that can stabilize a solar sail in the vicinity of an AEP. The design of AEPs that can enable new mission possibilities, using low-thrust propulsion, is documented in a large number of publications[1–3, 8, 17, 18]. However, the design of AEPs with solar sails usually assume that the solar sail is perfectly reflective. In Farrés [19] the dynamics of a solar sail in the Sun-Earth restricted three-body problem including specular reflection and absorption in the sail model is studied and periodic and quasi-periodic motions close to AEPs are computed. In this paper we consider a specular reflective and absorptive sail model since the RCD technology that we consider switch between these two states and assume that there is no diffuse reflection. Differently from an ideal sail, the SRP acceleration has a component along $\mathbf{n}$ and another along $\mathbf{s}$, which can be expressed as a single component vector along $\mathbf{m}$ (see Fig. 1). As a result, the vector product between the gradient of U (∇U) and $\mathbf{m}$ is zero (for an ideal sail ∇U is parallel to $\mathbf{n}$). Therefore, an AEP is defined as the location where $\mathbf{m}$ is

directed along the gradient of the pseudo-potential with $\mathbf{m}$ defined by

$$\mathbf{m} = \frac{-\nabla U}{\| - \nabla U \|} \tag{11a}$$

$$\tan\theta_L = \frac{\|\hat{\mathbf{r}}_1 \times -\nabla U\|}{< \hat{\mathbf{r}}_1, -\nabla U >} \tag{11b}$$

$$\tan\delta_L = \frac{\|(\hat{\mathbf{r}}_1 \times \hat{\mathbf{k}}) \times (\hat{\mathbf{r}}_1 \times -\nabla U)\|}{< (\hat{\mathbf{r}}_1 \times \hat{\mathbf{k}}), (\hat{\mathbf{r}}_1 \times -\nabla U) >} \tag{11c}$$

$$\beta = \frac{r_1^2}{(1-\mu)} \frac{\| - \nabla U \|}{\cos\alpha_L \sqrt{\rho_s \cos^2\alpha_L + (1-\rho_s)^2/4}} \tag{11d}$$

where θ_L, α_L, δ_L are respectively the effective cone angle, cone angle and clock angle of the AEP. α_L is obtained from θ_L by solving Eq. 3. The AEP is defined uniquely both in terms of position (x_L, y_L, z_L) and orientation (δ_L, α_L).

To design the orbit control, Eq. 7 are linearized in a neighborhood of a selected AEP (L_A) and written in the state-space domain: the state vector $\mathbf{x} = [\xi, \eta, \zeta]^T$ relative to L_A, while the control input vector $\boldsymbol{\theta} = [\alpha_c - \alpha_L, \delta_c - \delta_L]^T$ with the linearized dynamics expressed as

$$\dot{\mathbf{x}} = \mathbf{A}\,\mathbf{x} + \mathbf{B}\,\boldsymbol{\theta} \tag{12}$$

where $\mathbf{A} \in \mathbb{R}^{6\times6}$ and $\mathbf{B} \in \mathbb{R}^{6\times2}$ are the matrices $\mathbf{A}^*$ and $\mathbf{B}^*$ evaluated at the equilibrium point (x_L, y_L, z_L,δ_L, α_L) where:

$$\mathbf{A}^* = \begin{bmatrix} 0 & 0 & 0 & 1 & 0 & 0 \\ 0 & 0 & 0 & 0 & 1 & 0 \\ 0 & 0 & 0 & 0 & 0 & 1 \\ U_{xx}+a_{xx} & U_{xy}+a_{xy} & U_{xz}+a_{xz} & 0 & 2 & 0 \\ U_{yx}+a_{yx} & U_{yy}+a_{yy} & U_{yz}+a_{yz} & -2 & 0 & 0 \\ U_{zx}+a_{zx} & U_{zy}+a_{zy} & U_{zz}+a_{zz} & 0 & 0 & 0 \end{bmatrix}, \mathbf{B}^* = \begin{bmatrix} 0 & 0 \\ 0 & 0 \\ 0 & 0 \\ a_{x\alpha} & a_{x\delta} \\ a_{y\alpha} & a_{y\delta} \\ a_{z\alpha} & a_{z\delta} \end{bmatrix} \tag{13}$$

where U_{ij} and a_{ij} denote the partial derivatives with respect to i and j. A feedback control is then defined as $\boldsymbol{\theta} = -\mathbf{G}\,\mathbf{x}$ with $\mathbf{G} \in \mathbb{R}^{2\times6}$ defined as the control gain matrix which is computed using optimal control theory for linear time-invariant systems. This requires solving an algebraic Riccati equation and the approach is known as the

Linear Quadratic Regulator (LQR) control that minimizes the following cost function ($\mathcal{J}$)

$$\mathcal{J} = \frac{1}{2} \int_0^{+\infty} (\mathbf{x}^T \, \mathbf{Q} \, \mathbf{x} + \boldsymbol{\theta}^T \, \mathbf{R} \, \boldsymbol{\theta}) \, dt. \tag{14}$$

Here $\mathbf{Q} \in \mathbb{R}^{6\times6}$ is a non-negative, symmetric weighting matrix, and $\mathbf{R} \in \mathbb{R}^{2\times2}$ is a positive definite, symmetric weighting matrix. We note here that using this well-known LQR control is not essential for the pixelated RCD control. Indeed the ideal control can be changed to a more appropriate one defined by the control engineer. The useful output of the LQR control for the RCD control logic are the ideal acceleration $\mathbf{a} = [a_x \quad a_y \quad a_z]$ and the ideal cone and clock angles (α_c, δ_c). Moreover, a control design for the RCDs will be proposed that matches as close as possible the ideal acceleration while the cone and clock angles will be tracked using an attitude control.

B. Solar sail reduced attitude controller

The output cone and clock angles from the orbit control (δ_c, α_c) are used as inputs to define the reference angular velocity $\boldsymbol{\omega}_r$ and the reference pointing direction vector of the sail acceleration $\mathbf{b} = [\cos\alpha_c \quad \sin\alpha_c\cos\delta_c \quad \sin\alpha_c\sin\delta_c]^T$. Note that the desired attitude reference can be constructed from this vector and tracked. However, it is possible to use a reduced attitude control that only requires the desired pointing information. Our related conference paper [20] compared three ideal attitude controls: (i) A Proportional-Derivative control based on quaternions, (ii) an under-actuated control based on a complex attitude representation known as the $w - z$ parameters and (iii) the reduced-attitude or bore-sight control proposed by Pong and Miller [16]. The first two controls require a reference attitude while the bore-sight control only requires the desired pointing direction $\mathbf{b}$. The performance of the bore-sight control was shown to be superior to both the other controls in terms of tracking performance with one order of magnitude of control torque less than the proportional controller. We define the angle $\theta \in [0, \pi]$ between the normal to the sail $\mathbf{n}_B$ and the desired pointing direction $\mathbf{b}$, then the reduced control or bore-sight control is:

$$\mathbf{u} = \boldsymbol{\omega} \times \mathbf{J} \, \boldsymbol{\omega} + \mathbf{J} \, \dot{\boldsymbol{\omega}}_r - \mathbf{P} \, \mathbf{l} \, \sin\theta + \mathbf{D} \, \boldsymbol{\omega}_e \tag{15}$$

where $\mathbf{u}$ is the control torque vector, $\mathbf{J}$ is the moment of inertia tensor and $\mathbf{l}$ is a unit vector perpendicular to both $\mathbf{n}_B$ and $\mathbf{b}$. $\mathbf{P} = k_P \, \mathbf{J} \in \mathbb{R}^{3\times3}$ and $\mathbf{D} = k_D \, \mathbf{J} \in \mathbb{R}^{3\times3}$ are the proportional and the derivative gain matrices, respectively. k_P and k_D are scalar constant gains that are required to be tuned. $\boldsymbol{\omega}_r$ is the reference angular rate defined by [16]

$$\boldsymbol{\omega}_r = \omega_x(0) \, \mathbf{n}_B + \mathbf{b} \times \dot{\mathbf{b}} + \mathbf{b} \times (\boldsymbol{\omega} \times \mathbf{b}) \tag{16}$$

Finally, $\boldsymbol{\omega}_e = \boldsymbol{\omega}_r - \boldsymbol{\omega}$ represents the angular rate error. This control law has been proven to asymptotically track a desired pointing direction in [16]. Since the reduced attitude control can track the ideal attitude with a faster response

than the ideal orbit control, the coupled control will asymptotically stabilize the coupled orbit attitude dynamics. An additional benefit of this control for solar sail pointing is that it only requires the Sun direction (given by a Sun sensor) and the angular velocity (given by a gyro). The solar sail membrane itself could be used as a Sun sensor significantly reducing the sensor requirement and thus minimizing mass requirement. Note that the bore-sight control torque (Eq. 15) can be multiplied by a smoothing function $f = \left(1 - e^{-\epsilon\, t^2}\right)$ such that

$$\mathbf{u} = \left(1 - e^{-\epsilon\, t^2}\right) (\boldsymbol{\omega} \times \mathbf{J}\, \boldsymbol{\omega} + \mathbf{J}\, \dot{\boldsymbol{\omega}}_r - \mathbf{P}\, \mathbf{l}\, \sin\theta + \mathbf{D}\, \boldsymbol{\omega}_e). \tag{17}$$

where ϵ is a tuning parameter (selected as $5 \times 10^{-8}\,\mathrm{s}^{-2}$ in our simulations).Introducing f has the effect of reducing the large initial torques at the beginning of the simulation which cannot be matched sufficiently using RCDs.

IV. Reflectivity Control Devices

In this section we present an approach to map the ideal forces and torques from the ideal orbit and attitude controls to command each RCD to switch either on or off. The proposed approach significantly reduces the computational expense associated with computing and storing all the possible torques in a lookup table.

A. RCD-Based Attitude Control

In this section the attitude control based on distributed reflectivity control devices is described. Recall Eq. 5 which represents the torque acting on the sail due to SRP. Initially assume that the entire sail is one RCD then the SRP torque can be expressed as Eq. 5 becomes

$$\begin{cases} u_x &= P\, S\, \cos^2\alpha\, \tan\alpha\, (Z\, \cos\gamma + Y\, \sin\gamma)\, \kappa_x \\ u_y &= P\, S\, \cos^2\alpha\, Z\, \kappa_{yz} \\ u_z &= -P\, S\, \cos^2\alpha\, Y\, \kappa_{yz} \end{cases} \tag{18}$$

where the switching mode parameters are defined by

$$ON \quad \longrightarrow \quad \kappa_x = 0 \qquad \kappa_{yz} = 2 \qquad , \qquad OFF \quad \longrightarrow \quad \kappa_x = 1 \qquad \kappa_{yz} = 1 \tag{19}$$

Exploiting the symmetry of the sail we divide it into 4 quadrants as depicted in the left image of Fig. 3.

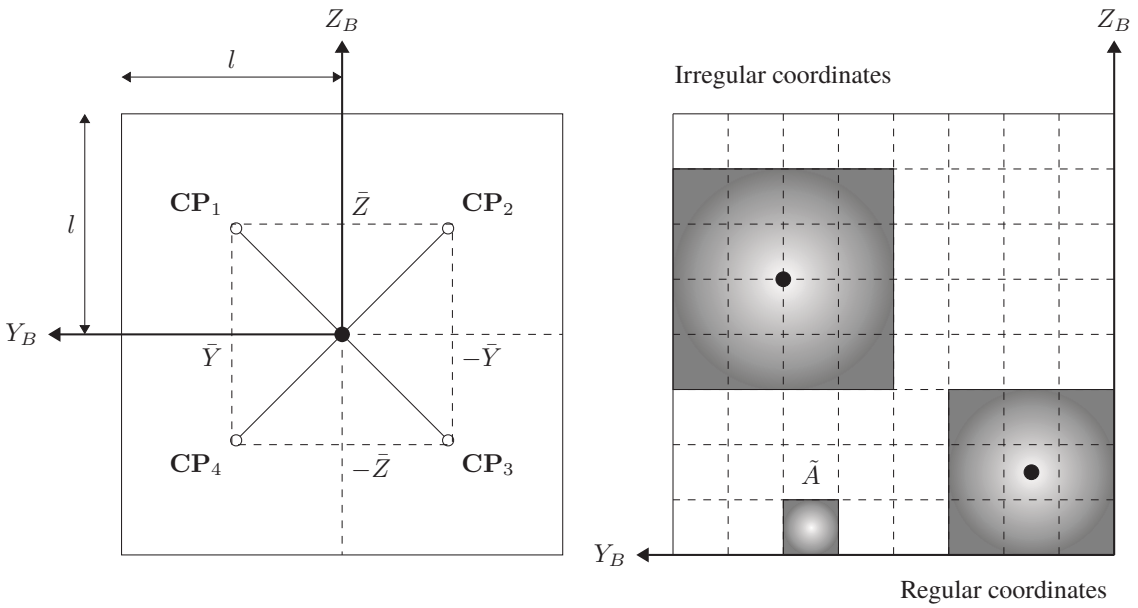

Fig. 3 Reflectivity control device-based attitude control logic scheme.

Initially consider each quadrant as a single RCD each with an assigned center of pressure $\mathbf{CP}_j$ ($j = 1, 2, 3, 4$). In the first stage of the control allocation assume each one has the same coordinate magnitudes ($\bar{Y}$, $\bar{Z}$) but with the respective signs as in Fig. 3. In this case $\bar{Y} = \bar{Z}$, since they are initialized in the centre. The torque generated by each quadrant has the same expression of Eq. 19 but with the appropriate value for the center-of-pressure and surface area. The overall torque generated by the four quadrants can then be expressed as:

$$\begin{cases} u_x &= P\,\bar{S}\,\cos^2\alpha\,\tan\alpha\,[\bar{Z}\,\cos\gamma\,(\kappa_x^1+\kappa_x^2-\kappa_x^3-\kappa_x^4)+\bar{Y}\,\sin\gamma\,(\kappa_x^1-\kappa_x^2-\kappa_x^3+\kappa_x^4)] \\ u_y &= P\,\bar{S}\,\cos^2\alpha\,\bar{Z}\,(\kappa_{yz}^1+\kappa_{yz}^2-\kappa_{yz}^3-\kappa_{yz}^4) \\ u_z &= -P\,\bar{S}\,\cos^2\alpha\,\bar{Y}\,(\kappa_{yz}^1-\kappa_{yz}^2-\kappa_{yz}^3+\kappa_{yz}^4) \end{cases} \tag{20}$$

where the superscript of the κ indicates the corresponding quadrant. The first stage of the proposed control allocation is to propose a simple method for choosing the 8 values of $\kappa_x^j, \kappa_{yz}^j$ where $j = 1, 2, 3, 4$. From Eq. 20 and for a fixed orientation of the sail κ_x^j and κ_{yz}^j can be selected to change the sign of the torque components u_y and u_z. While the sign of u_x depends also on the coordinates of the centre-of-pressure and on γ. Therefore, u_x is considered as a disturbing or parasitic torque that is not directly controlled. With four quadrants and two possible states (on/off) there are 16 possible combinations. This is used to select the parameters $\kappa_x^j, \kappa_{yz}^j$ based on the signs of the in-plane torque u_y, u_z. Among the 16 possibilities, only 8 different torques can be generated, as shown in Tab. 1. The combinations that include more "on" states have been chosen as this improves the ability to control the AEPs.

Using Table 1 we can select the values of $\kappa_x^j, \kappa_{yz}^j$ in Eq. (20) simply by observing the sign of the torques u_y, u_z,

Table 1 ON/OFF combinations with four quadrants.

Quadrants					
1	2	3	4	u_y	u_z
ON	ON	ON	OFF	> 0	> 0
ON	OFF	ON	ON	< 0	< 0
ON	ON	OFF	ON	> 0	< 0
OFF	ON	ON	ON	< 0	> 0
ON	ON	OFF	OFF	> 0	0
OFF	OFF	ON	ON	< 0	0
ON	OFF	OFF	ON	0	< 0
OFF	ON	ON	OFF	0	> 0

selecting the appropriate ON or OFF state and using Eq. (19).

1. Mesh Generation

Once the parameters $\kappa_x^j, \kappa_{yz}^j$ have been selected, the quadrants are pixelated in order to refine the control. Once the number of pixels has been chosen, the centre-of-pressure of each quadrant $\bar{Y}_j, \bar{Z}_j$ and the surface area of each quadrant $\bar{S}_j$ can be refined by switching pixels either ON or OFF. In order to simplify the control procedure the symmetry of each quadrant is preserved such that the total torque is still given by (20). Therefore, it is only necessary to select a single value of the surface area $\bar{S}_j = \bar{S}$ and symmetric coordinates such $\bar{Y}_j, \bar{Z}_j = \pm\bar{Y}, \pm\bar{Z}$. The first design step is to consider the order of the mesh of each quadrant $n \in \mathbb{N}$ which characterizes its precision. The order of the mesh n is defined in terms of the total number of RCDs, N_e, by the equation $N_e = 4^{n-1}$. The order of the mesh gives a, simple, small integer measure of the RCD sail precision. For example, as shown in Fig. 3 there are 64 RCDs and therefore the mesh has order 4. The area of each element ($\tilde{A}$) is related to n by $\tilde{A} = \frac{l^2}{2^{[2(n-1)]}}$ where l is the length of a quadrant. Note that the coordinates of the centers-of-pressure ($\bar{Y}_j$, $\bar{Z}_j$) can be either in the middle (regular) or the corner of an RCD (irregular) as shown in the right image of Fig. 3. In Fig. 3 the black dots represent different possibilities for the position of the centre-of-pressure. There is a need to differentiate between regular and irregular since the area $\bar{S}_j$ surrounding each consist of different multiples of a single element $\tilde{A}$. Moreover, for a regular element $\bar{S}_j$ is restricted to an odd multiple of $\tilde{A}$ explicitly given by $\bar{S}_j = (1 + 2(m-1))^2\tilde{A}$ where m is the number of layers of pixels about the centre of mass. For an irregular element $\bar{S}_j$ is restricted to even multiples of $\tilde{A}$ explicitly given by $\bar{S}_j = 4m^2\tilde{A}$.

The steps of the RCD-based attitude control are then

1) From the signs of the ideal in-plane torque choose the correct combination (Tab. 1) and associate the respective ON/OFF mode to each quadrant. This yields κ_x^j and κ_{yz}^j in Eq. 22.
2) Compute all the possible torques in Eq. 22 corresponding to all possible centres-of-pressure $\bar{Y}, \bar{Z}$ (regular and irregular) and all possible values of $\bar{S}$. These can be stored in a look-up table.

3) Select the $\bar{Y}, \bar{Z}, \bar{S}$ that minimizes the cost function

$$J = (u_y^{RCD} - u_y^{id})^2 + (u_z^{RCD} - u_z^{id})^2 \tag{21}$$

where (u_y^{id}, u_z^{id}) are the ideal in-plane torque components while (u_y^{RCD}, u_z^{RCD}) the one generated with the developed control.

4) Turn ON the pixels that correspond to $\bar{Y}, \bar{Z}, \bar{S}$ in the quadrants deemed ON from (1) and turn OFF the pixels that correspond to $\bar{Y}, \bar{Z}, \bar{S}$ in the quadrants deemed OFF from (1). All remaining pixels are switched ON as they will induce no net torque but maximize the sail performance for orbit control.

For example, consider the simple case of a sail oriented parallel to the Sun-sail line (i.e., $\alpha = 0\,\mathrm{deg}$). In this situation, for different orders of the mesh, the possible torques are shown in Fig. 4.

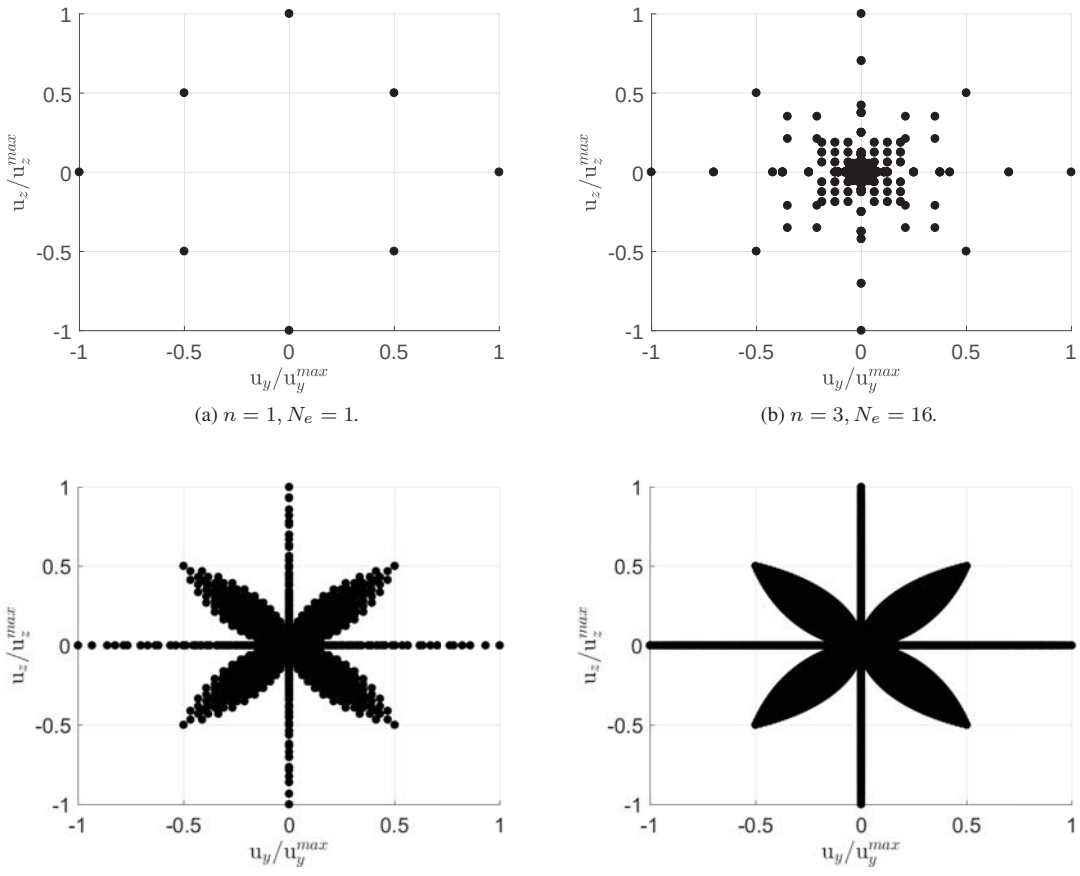

(a) $n = 1, N_e = 1$.

(b) $n = 3, N_e = 16$.

(c) $n = 5, N_e = 256$.

(d) $n = 7, N_e = 4096$.

Fig. 4 Available control torques relative to their maximum value ($\alpha = 0\,\mathrm{deg}$).

It can be seen that as n increases the majority of the torques form around the origin. Since the control will perform

better if the ideal torque is located within the black region, this implies that the control will work well if the ideal control is located close to the origin. This can be achieved by carefully tuning the ideal control so that the torques reside as close as possible to the black regions, while the black region can be increased by using more RCDs. However, increasing the number of RCDs significantly increases the computational expense, as pointed out in Ref. [15]. In any case, the optimization algorithm will try to match as best as possible the ideal torque with the possible torques generated by the RCDs i.e. a perfect matching of torques is not required.

B. RCD-Based Orbit Control

1. Orbit control

From the possible combinations there are those that do not produce any torque in the system: ON-OFF-ON-OFF, OFF-ON-OFF-ON, OFF-OFF-OFF-OFF. However, when an RCD is switched off it introduces a force that is not aligned completely with the sail normal. This result can be used to build a simple orbit control with the RCDs. The orbit control presented here is designed to mimic an ideal acceleration given by the LQR controller. In order to mimic the acceleration effectively, the sail in its nominal operating phase must include both specular reflective and absorptive components. Firstly, consider that in the attitude control design the number of RCDs that are switched off can be defined, and the ratio with respect to the total number of pixels computed (f_{OFF}). Defining f_{OFF}^{max} to be the maximum value of f_{OFF}, then, the value of ρ_s used in the orbital model of the sail is chosen such that $1-\rho_s > f_{OFF}^{max}$. This ensures that the ideal acceleration can always be achieved.

The steps for the orbit control based on RCDs are:

1) From the RCD-based attitude control, the total number of pixels switched on/off is known. So, the orbit control will have n_{max} remaining pixels to utilize. In addition, the pixels already used generate an acceleration related to the attitude control called $\mathbf{n}_B^A$.
2) Introduce the ideal acceleration $\mathbf{a}$ from the ideal orbit control (the LQR control). The required additional acceleration to mimic the ideal one is $\mathbf{a}^O = \mathbf{a} - \mathbf{a}^A$.
3) That acceleration must be given by the remaining pixels, that can be either switched on or off. The acceleration $\mathbf{a}^O$ is expressed in the synodic frame Sy. However, the relation is simpler if expressed in the L frame which can be achieved by matrix multiplication of $\mathbf{A}_{L/Sy}$:

$$\mathbf{A}_{L/Sy} = \begin{bmatrix} \hat{\mathbf{r}}_1^T \\ \left(\frac{(\hat{\mathbf{r}}_1\times\hat{\mathbf{k}})\times\hat{\mathbf{r}}_1}{\|(\hat{\mathbf{r}}_1\times\hat{\mathbf{k}})\times\hat{\mathbf{r}}_1\|}\right)^T \\ \left(\frac{\hat{\mathbf{r}}_1\times\hat{\mathbf{k}}}{\|\hat{\mathbf{r}}_1\times\hat{\mathbf{k}}\|}\right)^T \end{bmatrix} \tag{22}$$

Expressing the acceleration in the L frame and dividing by ($\mathbf{a}_L^{ON}$ and $\mathbf{a}_L^{OFF}$) gives

$$\mathbf{a}_L^O = \mathbf{a}_L^{ON} + \mathbf{a}_L^{OFF} = (n_{max} - n_{OFF})\ 2\ \frac{P\ \tilde{A}}{m}\ \cos^2\alpha\ \mathbf{n}_L + n_{OFF}\ \frac{P\ \tilde{A}}{m}\ \cos\alpha\ \mathbf{s}_L \tag{23}$$

n_{OFF} represents the even number of pixels to switch off computed by taking the square of the norm of Eq. 23. If the fraction of pixels switched off for orbit control with respect to the total number of pixels is introduced (f_O), the not-used fraction must be re-defined as $f_{NU} = 1 - (f_{ON} + f_{OFF} + f_O)$. The result will be that $f_{ON} + f_{NU} \longrightarrow \rho_s$ and $f_{OFF} + f_O \longrightarrow 1 - \rho_s$. In this case there is more than one way to decide what RCDs to switch OFF due to the fact that no torque is introduced. However, to induce no net torque each RCD chosen in the first quadrant, must be reflected about the axis of symmetry.

An example of orbit-attitude control mapped optimally in the pixels status, for $n = 4$, is shown in Fig. 5. Regarding the orbit control, all the three possible combinations have been used obtaining $n_{OFF} = 8$. In principle, the two combinations with 2 switched off pixels can be substituted by a single one with 4 switched off pixels.

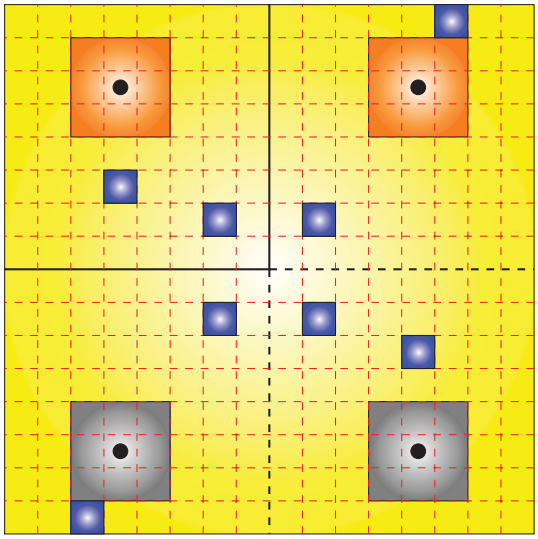

Fig. 5 Example of control, with pixels: yellow ⇒ ON not used, orange ⇒ ON for attitude control, grey ⇒ OFF for attitude control, blue ⇒ OFF for orbit control.

V. Simulations

In this section the proposed RCD orbit-attitude control is applied to drive a solar sail and maintain its position in the vicinity of an artificial L_1 point. The simulations are undertaken in the full-nonlinear orbit-attitude coupled equations of motion. The mass and sail area considered are that described in the Sunjammer mission [6] with the parameters listed in Tab. 2. The simulation is performed for $600\,\mathrm{d}$ with a fixed sample time of $10\,\mathrm{min}$ adopting a Bogacki-Shampine solver. The resulting trajectory and torques for the coupled orbit-attitude control are shown in Fig. 6. Fig 6a and 6b display

Table 2 Simulation parameters.

Parameter	Value
m	$45\,\mathrm{kg}$
S	$1444\,\mathrm{m}^2$
β	0.049344
J_x	$10\,830\,\mathrm{kg\,m}^2$
J	$5415\,\mathrm{kg\,m}^2$
ρ_s	0.9
x_L	$0.981\,406\,115\,03\,\mathrm{AU}$
y_L	$-0.002\,\mathrm{AU}$
z_L	$0.001\,805\,024\,04\,\mathrm{AU}$
δ_L	$19.287\,\mathrm{deg}$
α_L	$3.488\,\mathrm{deg}$
n	8
$\xi(0) = \zeta(0)$	$1000\,\mathrm{km}$
$\eta(0)$	$-1000\,\mathrm{km}$
$\dot{\xi}(0) = \dot{\eta}(0) = \dot{\zeta}(0)$	$1\,\mathrm{m\,s}^{-1}$
$\delta(0)$	$21\,\mathrm{deg}$
$\alpha(0)$	$6\,\mathrm{deg}$
$\gamma(0)$	$0\,\mathrm{deg}$
$\omega_x(0) = \omega_y(0) = \omega_z(0)$	$0\,\mathrm{rad\,s}^{-1}$
ν	1.5
$\mathbf{R}$	diag([1,1])
$\mathbf{Q}$	diag([10^5,10^5,10^5, 10^3,10^3,10^3])
k_P	$\pi^2 \times 10^{-8}\,\mathrm{rad\,s}^{-2}$
k_D	$20\,\sqrt{2}\,\pi \times 10^{-5}\,\mathrm{rad\,s}^{-1}$

the performance with an ideal control while Fig. 6c and Fig. 6d display the performance with the RCD control. Fig. fig:6e show the surface usage of the RCDs. The sail converges to the artificial equilibrium point with a precision in the order of $10^2\,\mathrm{m}$ as shown in Fig. 7. In addition it can be seen that the attitude angles converge to the desired ones (δ_L, α_L) in approximately $400\,\mathrm{d}$, with a precision in the order of $10^{-6}\,\mathrm{deg}$ as shown in Fig. fig:8. The attitude tracking of δ_c and α_c reaches steady-state after only $1\,\mathrm{d}$. Note that the trajectory of the RCD controller approximates the ideal controller closely in this example and the sail reaches a neighbourhood of the equilibrium point in the order of $10^1\,\mathrm{km}$. The tracking error of the desired attitude angles are of the order $\sim 10^{-3}\,\mathrm{deg}$ for δ and $10^{-4}\,\mathrm{deg}$ for α.

Fig. 9 shows the different trajectories of the RCD sail for an increasing value of n. For $n = 5$ (Fig. 9a and 9b) the sail does not reach a neighbourhood of L_A. For $n = 6$ (Fig. 9c, 9d, 9e and 9f) the sail approaches the AEP, although the tracking of the angles is not precise. Recall from Fig. fig:6c and Fig. fig:6d that for $n = 8$ the sail tracks the AEP with a precision in the order of $10^2\,\mathrm{m}$. Fig. 10a displays the local surface usage in the first $15\,\mathrm{h}$. For $n = 5$ (Fig. 10a) the

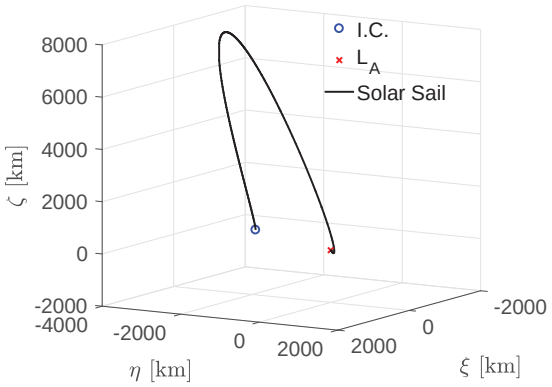

(a) *Ideal trajectory.*

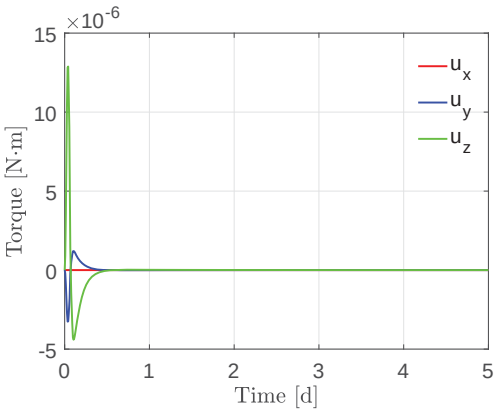

(b) *Ideal control torque.*

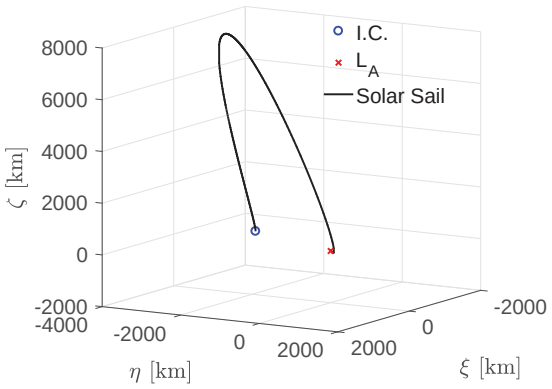

(c) *Real trajectory.*

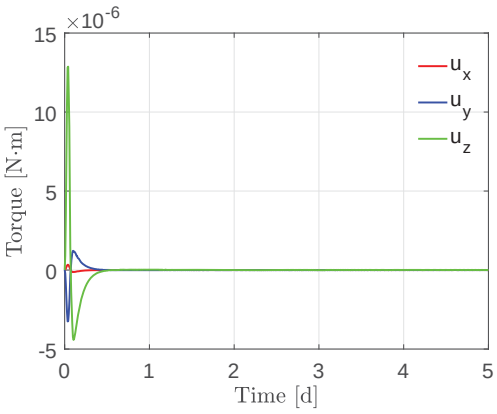

(d) *Real control torque.*

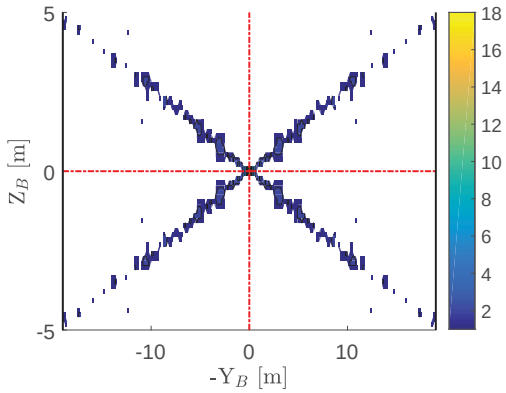

(e) *Local surface usage for attitude control:* $0 - 15$ h.

Fig. 6 Coupled dynamics simulations.

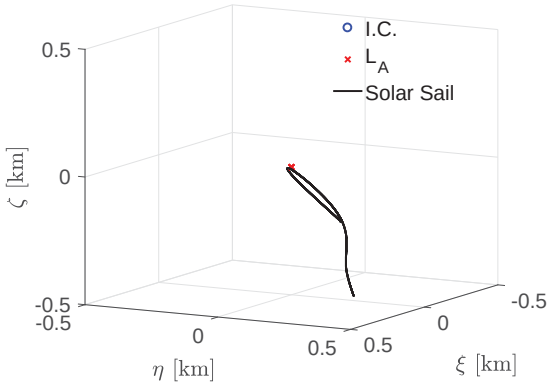

(a) *Fig 6.a zoomed in to show the trajectory converging to a neighbourhood of the desired point to within 10 km.*

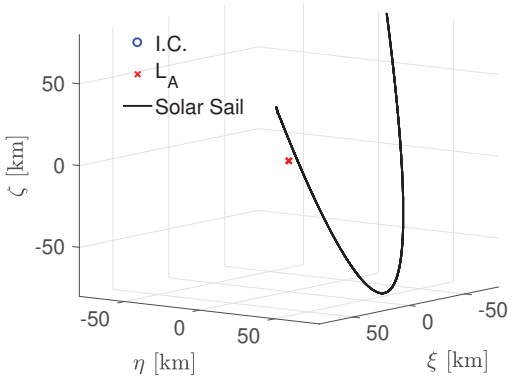

(b) *Fig 6.c zoomed in to show the trajectory converging to a neighbourhood of the desired point to within 10 km.*

Fig. 7 Trajectory converging to a region of the equilibrium point

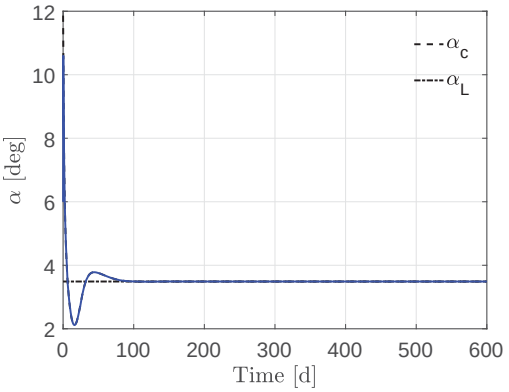

(a) α *over 600 days.*

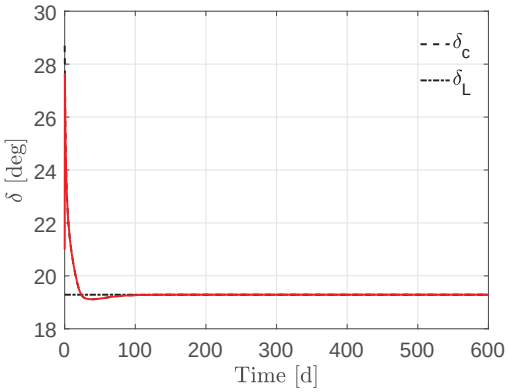

(b) δ *over 600 days.*

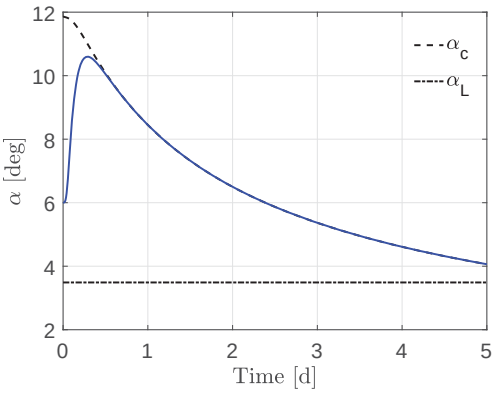

(c) α *over 5 days.*

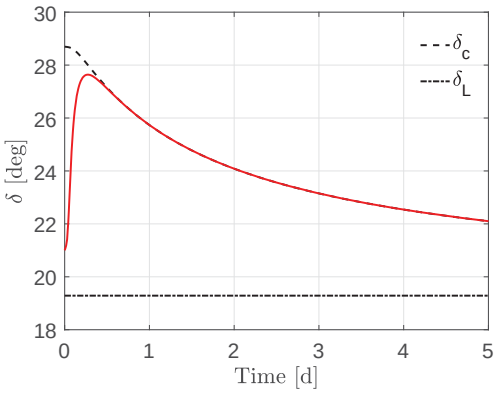

(d) δ *over 5 days.*

Fig. 8 Solar sail cone and clock angles over time

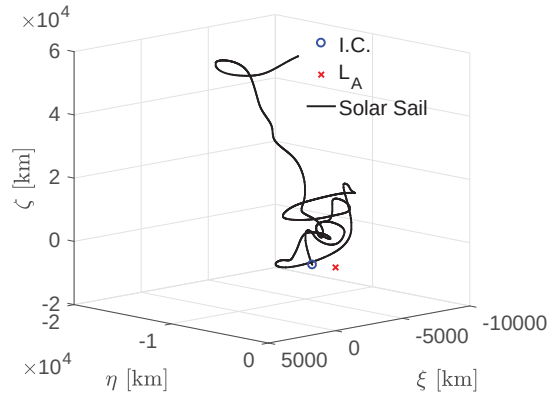

(a) *Trajectory with* $n = 5$.

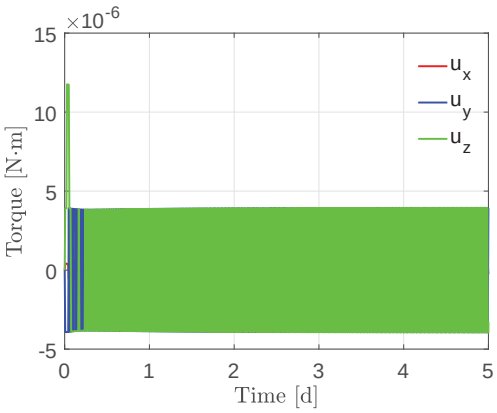

(b) *Control torque with* $n = 5$.

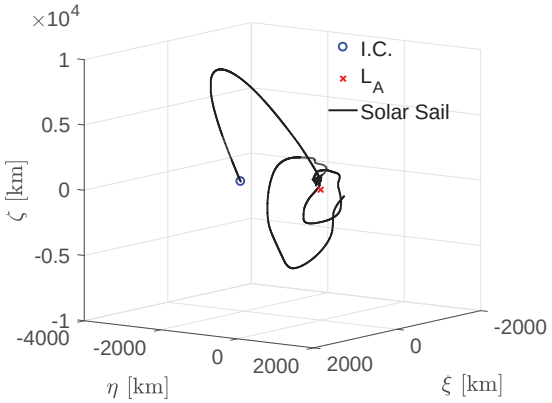

(c) *Trajectory with* $n = 6$.

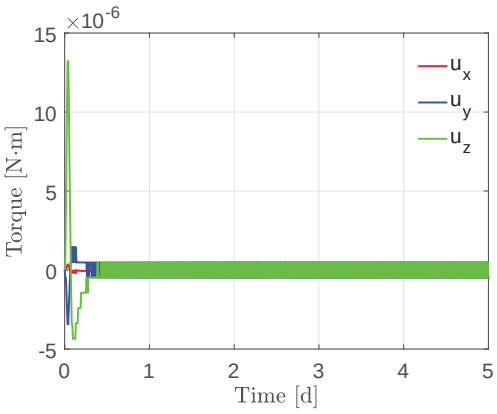

(d) *Control torque with* $n = 6$.

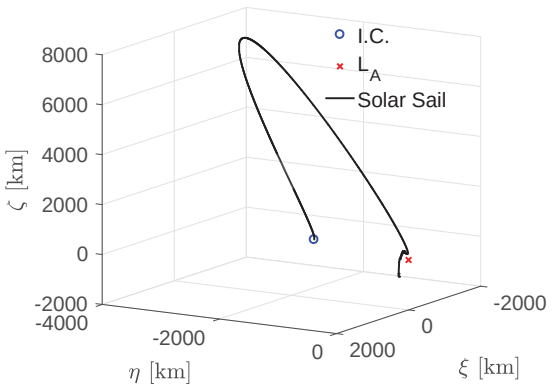

(e) *Trajectory with* $n = 7$.

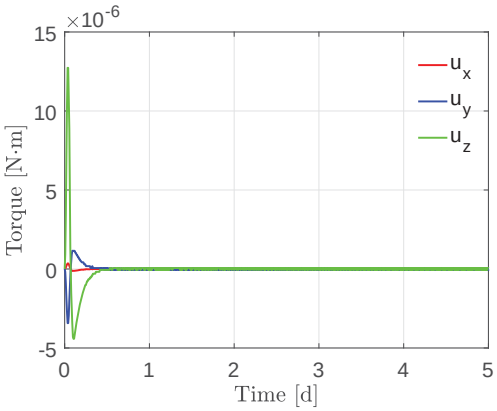

(f) *Control torque with* $n = 7$.

Fig. 9 Coupled dynamics dependence on n.

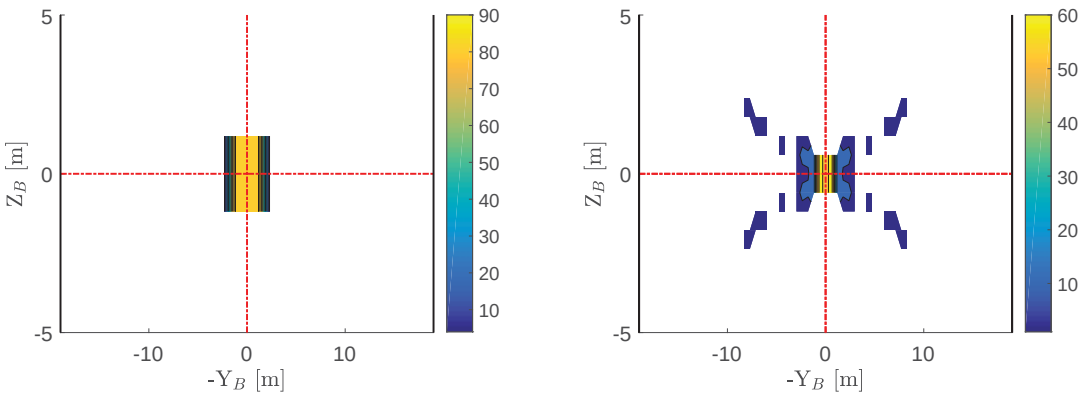

(a) $n = 5$.

(b) $n = 6$.

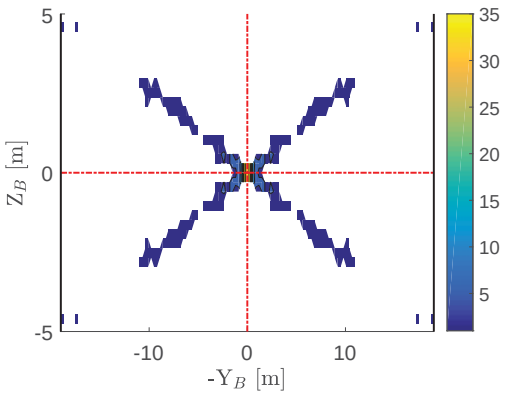

(c) $n = 7$.

Fig. 10 Local surface usage $(0 - 15\ \mathrm{h})$ **dependence on the mesh precision** n**.**

central pixels are always used. However, increasing n it can be seen that the ideal torque is mimicked with greater precision (Fig. 10b and 10c).

VI. Conclusion

This paper proposes an orbit-attitude tracking control based on distributed reflectivity control devices (RCDs). The orbit and attitude dynamics are coupled through the use of RCDs since they induce both a force and a torque. The control allocation which maps an ideal control to the ON or OFF mode of each RCD reduces the computational expense when compared to algorithms which compute all possible torques with every possible combination of RCDs. With enough RCDs covering the sail surface the tracking of an artificial equilibrium point in the solar sail circular restricted three body problem can be achieved. Moreover, as the number of RCDs on the sail membrane increases the ability to mimic an ideal torque increases. It is shown that for a sail of 1444 m^2 weighing $45kg$ that over 16,000 RCDs would be required to cover the sail surface to achieve convergence to a neighbourhood of an equilibrium point in the order of 10^2 m. Using RCDs, therefore, offer a potential means of controlling both the attitude and orbit of a solar sail in deep-space and have the advantage that they do not require mechanical actuation, are low mass and fuel-free.

References

[1] McKay, R., Macdonald, M., Biggs, J., and McInnes, C., "Survey of highly non-Keplerian orbits with low-thrust propulsion," *Journal of Guidance, Control, and Dynamics*, Vol. 34, No. 3, 2011, pp. 645–666. doi:10.2514/1.52133.

[2] Heiligers, J., Ceriotti, M., McInnes, C. R., and Biggs, J. D., "Mission analysis and systems design of a near-term and far-term pole-sitter mission," *Acta Astronautica*, Vol. 94, No. 1, 2014, pp. 455–469. doi:10.1016/j.actaastro.2012.12.015.

[3] Heiligers, J., Diedrich, B., Derbes, B., and McInnes, C. R., "Sunjammer: Preliminary End-to-End Mission Design," *2014 AIAA/AAS Astrodynamics Specialist Conference*, San Diego, California 2014. AIAA/AAS paper 2014.

[4] Mu, J., Gong, S., and Li, J., "Coupled Control of Reflectivity Modulated Solar Sail for GeoSail Formation Flying," *Journal of Guidance, Control, and Dynamics*, Vol. 38, No. 4, 2015, pp. 740–751. doi:10.2514/1.G000117.

[5] Borggräfe, A., Heiligers, J., Ceriotti, M., and McInnes, C. R., "Optical Control of Solar Sails using Distributed Reflectivity," *Spacecraft Structures Conference*, National Harbor, Maryland, January 2014. AIAA paper 2014-0833.

[6] Tamakoshi, D., and Kojima, H., "Solar Sail Orbital Control Using Reflectivity Variations near the Earth–Moon L_2 Point," *Journal of Guidance, Control, and Dynamics*, Vol. 41, No. 2, 2018, pp. 417–430. doi:10.2514/1.G002679.

[7] Gao, C., Yuan, J., Zhang, J., and Guo, L., "Propellant-efficient station-keeping using a hybrid sail in the Earth-Moon system," *Non-linear Dynamics*, November 2018. doi:10.1007/s11071-018-4631-1.

[8] Bookless, J., and McInnes, C., "Control of Lagrange point orbits using Solar Sail propulsion," *Acta Astronautica*, Vol. 62, No. 1, 2008, pp. 159–176.

[9] Waters, T., and McInnes, C., "Invariant Manifolds and Orbit Control in the Solar Sail Three-Body Problem," *Journal of Guidance, Control, and Dynamics*, Vol. 31, No. 3, 2008, pp. 554–562. doi:10.2514/1.32292.

[10] Biggs, J., McInnes, C., and Waters, T., "Control of solar sail periodic orbits in the elliptic three-body problem," *Journal of Guidance, Control, and Dynamics*, Vol. 32, No. 1, 2009, pp. 318–320. doi:10.2514/1.38362.

[11] Biggs, J., and McInnes, C., "Solar sail formation flying for deep-space remote sensing," *Journal of Spacecrafts and rockets*, Vol. 46, No. 3, 2009, pp. 670–678. doi:10.2514/1.42404.

[12] Wie, B., *Space Vehicle Dynamics and Control*, 2nd ed., AIAA Education Series, American Institute of Aeronautics and Astronautics, Reston, VA, USA, 2008.

[13] Takao, Y., Mori, O., and Kawaguchi, J., "Interplanetary Mission Design for Spinning Solar Sails Utilizing Active Shape Control of Sail Membranes," *2018 Space Flight Mechanics Meeting*, Kissimmee, Florida, January 2018. AIAA paper 2018-0212.

[14] Saiki, T., Tsuda, Y., Funase, R., Mimasu, Y., and Shirasawa, Y., "Attitude Operation Results of Solar Sail Demonstrator IKAROS," *Proceedings of the 28th ISTS (International Symposium on Space Technology and Science)*, Okinawa, Japan, June 5-12, 2011.

[15] Borggräfe, A., Heiligers, J., Ceriotti, M., and McInnes, C. R., "Attitude Control Of Large Gossamer Spacecraft Using Surface Reflectivity Modulation," *65^{th} International Astronautical Congress*, Toronto, Canada, September 2014, pp. IAC–14.

[16] Pong, C. M., and Miller, D. W., "Reduced-Attitude Boresight Guidance and Control on Spacecraft for Pointing, Tracking, and Searching," *Journal of Guidance, Control, and Dynamics*, Vol. 38, No. 6, 2015, pp. 1027–1035. doi:10.2514/1.G000264.

[17] McInnes, C. R., *Solar Sailing - Technology, Dynamics and Mission Applications*, Springer-Praxis Books in Astronautical Engineering, Springer and Praxis, Chichester, UK, 1999.

[18] Macdonald, M., McKay, R., Vasile, M., Bosquillon De Frescheville, F., Biggs, J. D., and McInnes, C., "Low-thrust-enabled highly-non-Keplerian orbits in support of future Mars exploration," *Journal of Guidance, Control, and Dynamics*, Vol. 34, No. 5, 2011, pp. 1396–1411. doi:10.2514/1.52602.

[19] Farrés, A., "Catalogue on the Dynamics of a Solar Sail around L1 and L2," *International Symposium on Solar Sailing 2017*, Kyoto, Japan, 2017.

[20] Negri, A., and Biggs, J. D., "Attitude Tracking of a Solar Sail Using Pixelated Reflectivity Control Devices," *International Symposium on Solar Sailing 2019*, Aachen, Germany, 2019.